Holiday-Inn Waterfront Hotel Kingston, Ontario, Canada, 2013 September 15-18



THE EFFECT OF OXIDIZED UO₂ ON IODINE-INDUCED STRESS CORROSION CRACKING OF FUEL SHEATHING

A.D. Quastel¹, E.C. Corcoran² and B.J. Lewis³

¹Atomic Energy Canada Ltd., Chalk River, Ontario, Canada

(Tel: 613-584-8811 x. 44812, quastela@aecl.ca)

²Royal Military College of Canada, Kingston, Ontario, Canada

³University of Ontario Institute of Technology, Oshawa, Ontario, Canada

ABSTRACT: In this study, axially-slotted Zircaloy-4 rings prepared from CANDU-type sheathing were stressed and inserted into glass-blown tubes with iodine crystals. Iodine quantities per total Zircaloy-4 surface area ranged from 4.2±0.2 mg cm⁻² to 35.5±0.7 mg cm⁻². Glass tubes were evacuated of air, sealed, and inserted into a tube furnace at 350°C to simulate the temperature of the fuel-to-sheath gap. The extent of specimen corrosion was assessed by observing stress corrosion cracking failures or when no cracking occurred, by measuring specimen deflections. Results show that the corrosion resistance of Zircaloy-4 to iodine species, which is Zircaloy texture dependent, increased when additives of: i) oxygen gas; and ii) hyperstoichiometric UO₂ with dried graphite were included in the glass ampoule. The latter suggests a chemical role of CANLUB in mitigating stress corrosion cracking in fuel sheathing.

Introduction

Iodine-induced stress corrosion cracking (I-SCC) is usually the cause of pellet-cladding interaction (PCI) failures of the unlined Zircaloy cladding surrounding the UO₂ reactor fuel pellets [1]. PCI can occur when the expanding and cracked fuel pellets make contact with the cladding of boiling or pressurized water reactor (BWR and PWR) fuel or collapsed sheathing in CANDU fuel. PCI failures usually occur in fuel rods with a burnup of over 10 GWd (tUO₂)⁻¹ during rapid power ramps. Generally, the conditions for I-SCC failure depend on: i) the critical stress (and strain) in the sheath/clad; ii) critical iodine concentration; and iii) the minimum amount of time the clad is stressed [1].

During reactor operation, the concentration of iodine inside the fuel element increases. With power ramps, the ceramic fuel can crack and expand further, and with sheath/clad contact, the sheath/clad hoop stress can increase and reach the yield point. If the fission products leave the fuel grains, they can migrate along the fuel cracks and reach the inside surface of the Zircaloy sheath. With chemical and mechanical interactions present, I-SCC failures can occur in the sheathing near the radial cracks in the fuel pellet [2] [3].

Fission-product iodine in nuclear fuel is not the only element that can cause SCC in Zircaloy sheathing. For instance, cesium/cadmium vapors have initiated corrosion in the form of a liquid metal embrittlement process [4] [5]. In fact, since the total production of cesium is ten times larger than that of iodine in the fuel element [1] and because iodine reacts with cesium to form stable CsI [6], it was initially believed that not enough iodine would be available for SCC. However, research has shown that CsI on its own does not sufficiently cause SCC in the Zircaloy [6]. Instead, in the presence of radiation, CsI can be dissociated to release iodine that causes cracking [6] [7]. Fractographic evidence [2] [5] has shown that the stress corrosion cracking in

fuel sheathing with iodine is usually a combination of both intergranular (IG) and transgranular (TG) cracking, whereas the cracking in cesium/cadmium vapors is always TG. Consequently, the observed PCI cracks in CANDU fuel are usually a combination of both IG and TG cracking, in which iodine is believed to be the main cause of SCC in Zircaloy sheathing [2] [5]. Hence, iodine is usually the species of interest in most SCC studies involving Zircaloy in nuclear fuel.

Historically, PCI failures were first observed in the 1960's in BWRs, and in the 1970's in CANDU reactors. To reduce the effects of PCI, BWR fuel adopted a pure zirconium barrier (i.e., a 'liner') and Canadian reactors introduced a thin layer of graphite called 'CANLUB' on the inside surfaces of the Zircaloy sheathing from 1970-1980. The graphite layer was believed to act as a lubricant, which decreases the coefficient of friction between the expanding fuel pellets and the collapsing sheath [8]. It has also been suggested that graphite impurities may act as a getter for iodine [7].

With the successful incorporation of the graphite layer and implementation of strict reactor operating parameters, development of other PCI mitigation techniques in CANDU fuel has received little attention, except for situations during power transient [3] [9]. However, further study on PCI mitigation is required to facilitate the design of load-following reactor operation and possibly for new reactor builds, which could utilize higher burn-up for increased fuel economy. This study focuses on investigating whether the graphite coating has chemical functionality beyond its originally perceived physical role as a fuel-to-sheath stress reducer. Specifically, it is useful to determine if a chemical interaction exists between the Zircaloy, graphite, and oxygen partial pressure (controlled by: (i) an oxygen gas addition, and (ii) the inclusion of hyperstoichiometric UO₂) to further understand the PCI process.

1. Chemistry of I-SCC

I-SCC can be initiated when the bare Zircaloy metal is exposed to corrosive iodine and tensile stress. Fortunately, in the absence of large stresses, a naturally occurring oxide layer (Eq. (1)) initially protects the Zircaloy from corroding [10]. However, in the presence of stress, the oxide layer will crack, exposing the bare underlying metal, which can initiate cracking and subsequent corrosion of the metal.

$$Zr(s) + O_2(g) \rightarrow ZrO_2(s, monoclinic)$$
 $\Delta G = -977 \text{ kJ at } 623 \text{ K and } 1 \text{ atm}$ (1)

It is believed that a small oxygen partial pressure (or oxidizing species) may assist in repairing breaches in the oxide layer, thereby reducing I-SCC. During normal operating conditions, excess oxygen is generated in irradiated fuel. At 1 atomic percent (at%) burnup, the excess oxygen per at% burnup can increase the oxygen-to-metal (O/M) ratio in UO₂ fuel from 2.000 to 2.009 [11]. Post-irradiation examinations have shown that the oxygen balance in irradiated fuel appears to be in the near stoichiometric region [11], indicating the presence of a possible reducing agent. Other work [12] shows that, without a reducing agent, the decomposition of U₃O₈ usually stops at UO_{2.15} (which is not stoichiometric UO₂) when in a vacuum of 20 mTorr or less of oxygen and at temperatures up to 1300°C. In the same work, it was claimed that UO₃ can be reduced with

CO to produce UO_2 at 350°C. Hence, it is possible for UO_{2+x} in CANDU fuel to be reduced by carbon from the graphite coating to produce carbon monoxide and carbon dioxide. Eq. (2) describes this reaction when, for example, x = 0.05 (where x is the deviation from UO_2 stoichiometry). The Gibbs free energy change for this solid state reaction was calculated using FactSage $6.1^{\$}$ Gibbs energy minimization software [13].

$$2UO_{2.05}(s) + 0.05C(s) \rightarrow 2UO_2(s) + 0.05CO_2(g)$$
 where $\Delta G = -2.31x10^3$ kJ at 623 K and 1 atm (2)

Since ΔG is negative, the reaction is thermodynamically favourable. Oxygen may also be available in the oxygen and carbon reaction as:

$$2CO(g) + O_2(g) \leftrightarrow 2CO_2(g)$$
 where $\Delta G = -457 \text{ kJ}$ at 623 K and 1 atm (3)

The negative value in Gibbs energy in Eq. (3) indicates a product-favoured reaction, so the gaseous oxygen concentration will be low. Since the produced carbon dioxide gas moves freely in the fuel element via the fuel cracks in pellet-pellet gaps and the fuel-to-sheath gap, it may make contact with the sheathing and oxidize any bare zirconium metal where the zirconium oxide layer has been damaged previously by cracking. Eq. (4) describes this reaction.

$$Zr(s) + CO_2(g) \rightarrow ZrO_2(s, monoclinic) + C(s, graphite) \Delta G = -582 \text{ kJ mol}^{-1} \text{ at } 623 \text{ K}$$
 (4)

A thermodynamic computation similar to Eq. (4) could be conducted where carbon monoxide is the reactant. If the chemical processes described above are taking place in CANDU fuel, they may help to explain the benefits of the graphite in reducing the occurrence of PCI failures.

The study reported in this paper used slotted ring specimens of Zircaloy-4 fuel sheath in I-SCC experiments with a similar test setup as considered by Wood [14]. New experimental techniques were incorporated and oxygen and hyperstoichiometric UO₂ were also included to investigate their effect on the corrosion behaviour of Zircaloy-4 with iodine.

2. Experimental

2.1 Materials

Slotted ring specimens were prepared from two types of Zircaloy-4 sheathing. The identification number and dimensions of each specimen type are outlined in Table 1. The first specimen type (28-element fuel bundle type) was provided as ready-cut individual specimens by Chalk River Laboratories. The second specimen type was prepared from current ~480 mm long, 37-element CANDU-6 fuel sheathing, manufactured by Cameco Fuel Manufacturing. Individual ring specimens were cut and slotted from these sheaths using a Buehler ISOMET 1000 Precision Saw with a UKAM Industrial diamond blade.

Table 1: Identification and dimensions of Zircaloy-4 slotted ring specimens								
						Wall thickness	Axial wid	

Specimen type #	Identification number	OD [mm]	Wall thickness t [mm]	Axial width <i>l</i> [mm]
1) Pickering 28-element type sheath (early type)	MLI-790, 7A3-393-4A	15.50±0.25*	0.40±0.01	5.0±0.1
2) CANDU-6 37-element type sheath	248389-5 DAC 18787	13.10±0.05	0.40±0.01	5.0±0.1

^{*}Measurement recorded from as-received specimens.

2.2 Stress wedges

To simulate the stress, two Zircaloy-4 wedge configurations were used to impart stress on Zircaloy ring specimens: i) a static wedge (ST); and ii) impact-tightened in-situ sliding wedge (SW). When a slotted ring is stressed using a wedge (Figure 1a), the maximum tensile transverse stress occurs directly opposite the wedge on the inner ring surface (Figure 1b). The maximum transverse stress imparted in the slotted ring due to the wedge is [14]:

$$\sigma_{transverse} = \frac{Et(w-b)}{3\pi R^2} \tag{5}$$

where E (Pa) is the Young's modulus of Zircaloy [15], t (m) is the slotted ring thickness (exaggerated in Figure 1b), w (m) is the wedge thickness, b (m) is the initial slot width before installing the wedge (not the width of the diamond blade), and R (m) is the radius of the slotted ring to its neutral axis (dashed curve in Figure 1b). The stress profile through the slotted ring wall is similar to a loaded beam (i.e., half tensile and half compressive through the beam cross-section with a neutral axis at its mid-wall location).

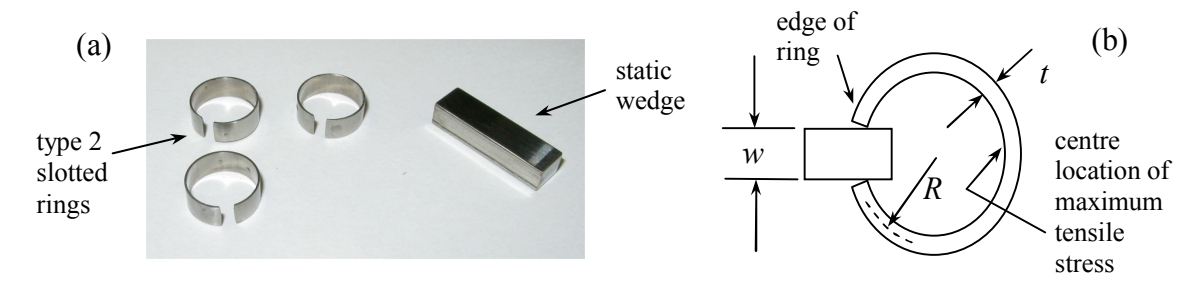


Figure 1: (a) Zircaloy slotted rings and a static wedge prepared for I-SCC testing, and (b)

Stress-loading of a slotted ring using a wedge (figure not to scale)

The second wedge configuration is the sliding wedge pair, shown in Figure 2a before use. In Figure 2b two slotted rings installed on the sliding wedge pair are shown prior to in-situ impact tightening. The Zircaloy sliding wedges were designed to tighten and lock when made to fall and impact (a number of times) on one end in a glass ampoule. These wedges apply stress to disturb the oxide layer in an oxygen-free environment, which prevents the reformation of oxide

on the newly exposed metal. A typical initial Zircaloy-4 oxide layer thickness when exposed to air at room temperature is ≈ 4 nm [16], or about 15 monolayers.

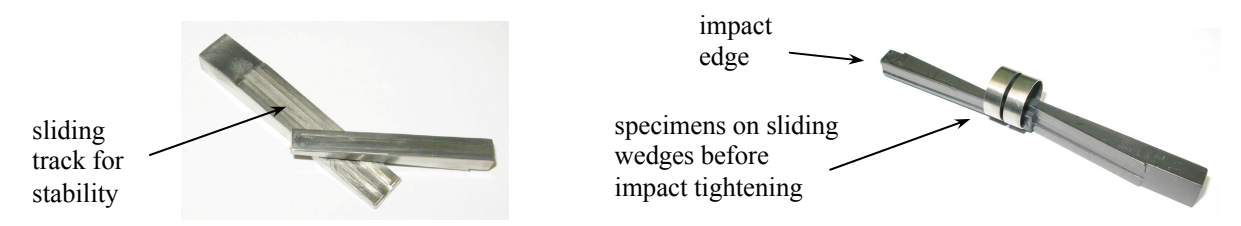


Figure 2: (a) Zircaloy sliding wedges, and (b) slotted ring specimens installed on sliding wedges before in-situ impact tightening

2.3 X-ray diffraction

The sheathing crystallographic texture influences its susceptibility to I-SCC [17]. Specifically, increased I-SCC resistance is achieved when the basal plane normal is parallel to the radial direction of the sheath. Radial normal sections of two specimen types were analyzed using a Scintag X-ray diffractometer. Figure 3 provides the scan of a Type-1 specimen and shows a dominant pyramidal plane $(2\overline{1}13)$ at 36.5°. Two other planes that can be noted in the scan are the basal plane (0002) at 34.8° and a prism plane $(11\overline{2}0)$ at 56.9° (which is a main slip plane and a Type II prism plane, respectively) [18].

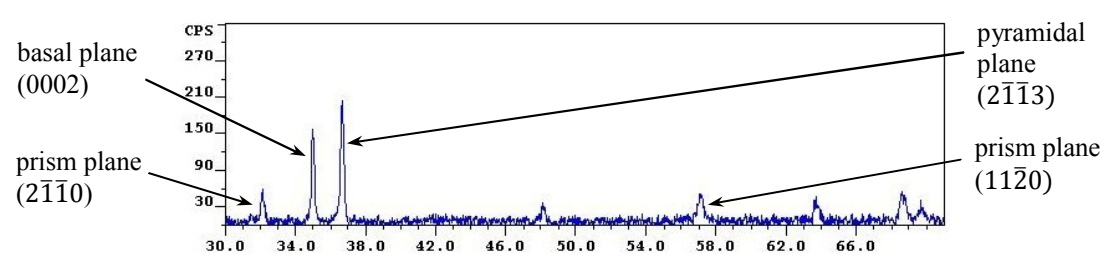


Figure 3: XRD diffraction scan of Type-1 slotted ring specimen material (showing less basal radial texture)

Figure 4 provides a scan of a Type-2 specimen. Here, the basal plane is the dominant peak and the pyramidal plane is reduced. One also notices that prism planes $(11\overline{2}0)$ and $(2\overline{1}10)$ are absent. As will be discussed, texture has an effect on the corrosion resistance of the samples.

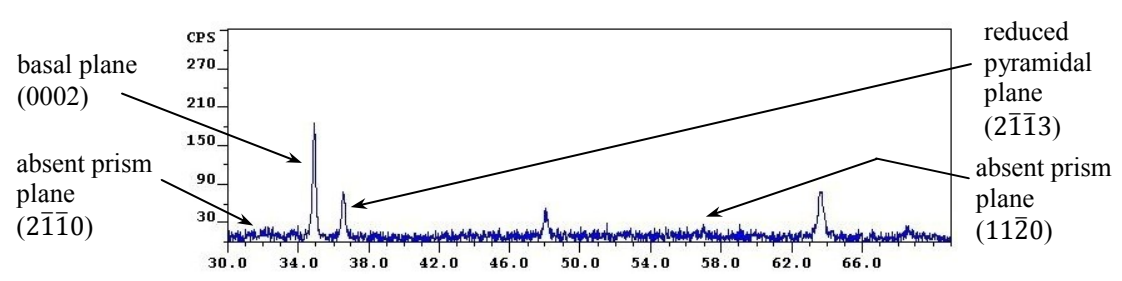


Figure 4: XRD diffraction scan of Type-2 slotted ring specimen material (showing more basal radial texture)

2.4 Experimental procedure

The experimental setup consisted of Zircaloy slotted rings that were pre-loaded using a Zircaloy wedge (Figures 1 and 2). At room temperature, the maximum applied stress in both types of slotted ring specimens, calculated using Eq. (4), was 480 ± 10 MPa. Figure 5 shows a static wedge being used. The loaded Type-1 specimens were inserted in a 2.47 cm ID Pyrex tubing that was 14-18 cm long and Type-2 specimens were inserted in 2.05 cm ID Pyrex tubing that was 22-24 cm long, which were glass blown shut at one end. Also inserted into the glass tube was a glass vial containing iodine crystals. In certain experiments, a mixture of UO_{2+x} (87-141 mg) and graphite (CANLUB DAG154N) (255-278 mg), the latter previously baked in air and then in vacuum, was also introduced as shown in Figure 5.

The UO_{2+x} was prepared by heating and weighing initially stoichiometric uranium dioxide in a Setaram Instrumentation SETSYS Evolution thermogravimetric analyzer. The material was initially reduced with a 2% H_2 and Ar carrier gas at 1273 K, and then oxidized with a 0.2% H_2 and Ar carrier gas with a low level of oxygen supplied by a Zirox SGM5EL electrolysis device. The stoichiometric deviation achieved for these tests ranged from x = 0.06 to 0.16. In other tests, 0.006-0.06 atm of pure oxygen gas was introduced in the glass ampoule vacuum by using a needle valve and diaphragm vacuum gauge.

Since oxygen in air reacts with zirconium to form a thin protective oxide layer [10] [19] (see Eq. (1)), a vacuum system was used to remove all air and moisture. The vacuum system consisted of an Alcatel 2005 Pascal Dual Stage rotary vane roughing pump and a Varian V70D turbo molecular pump. The pumping time typically took between 18-24 hours to achieve a vacuum pressure of 7-30 μ Torr. The glass tube was then glass blown shut with the vacuum maintained, effectively sealing in the components of the experiment in the prepared glass



Figure 5: Sealed glass ampoule with pre-stressed Zircaloy specimens, iodine glass vial corrodant and UO_{2+x} and dried graphite additive

ampoule. Once all the components were sealed in the evacuated glass ampoule, the iodine glass vial was broken by gentle agitation. Iodine had been placed in its own glass vial to prevent the loss of iodine to sublimation during the vacuum pumping and glass blowing (heating) stages. This setup avoided potential damage to the pumping equipment.

At this point, the glass ampoule was inserted into a MTI OTF-1200X 2.5kW tube furnace pre-set to 350±1°C to replicate the approximate temperature in a fuel-to-sheath gap. During the first 15 minutes to several hours, the iodine crystals in the glass vial completely sublimated into a dark purple vapor. During this time, the iodine reacted with the zirconium to form ZrI, ZrI₂, ZrI₃

and ZrI₄ [1] [7]. These deposits were later analyzed using Energy-Dispersive X-ray spectroscopy (EDX) and Nuclear Activation Analysis (NAA) at RMC to determine the chemical element composition. At a certain time (minutes to hours into the test), the purple iodine vapor quickly dissipated leaving behind orange/brown ZrI_x deposits (salts). The glass ampoule was heated continuously for five days. During this time, the specimens were visibly inspected from time to time through the glass ampoule for signs of obvious failure. This entailed pushing the glass ampoule out of the furnace momentarily and then pushing it back in.

Once the heating period was completed, the specimens were removed from the glass ampoule by breaking the glass ampoule at one end. Specimens were carefully removed from the wedges and dropped into an ethanol-filled beaker and gently stirred to remove deposits and eroded zirconium iodide materials.

For cases where the slotted ring specimens remained intact, a slotted ring deflection tester was designed and built to measure the extent of corrosion and cracking. Deflection measurements at room temperature were taken from minutes to weeks after the test. Figure 6 shows a photograph of the deflection tester. A slotted ring specimen was attached to the static and lever jaws while, at the other end, a 50 g weight was attached to deflect the specimen. An OMEGA LD400-1 linear displacement transducer detected the vertical displacement of the specimen. The transducer was powered by a HP 6236B power supply and a National Instruments NI 9205 data acquisition card in a NI cDAG-9172 chassis, connected to a computer running LabView, which

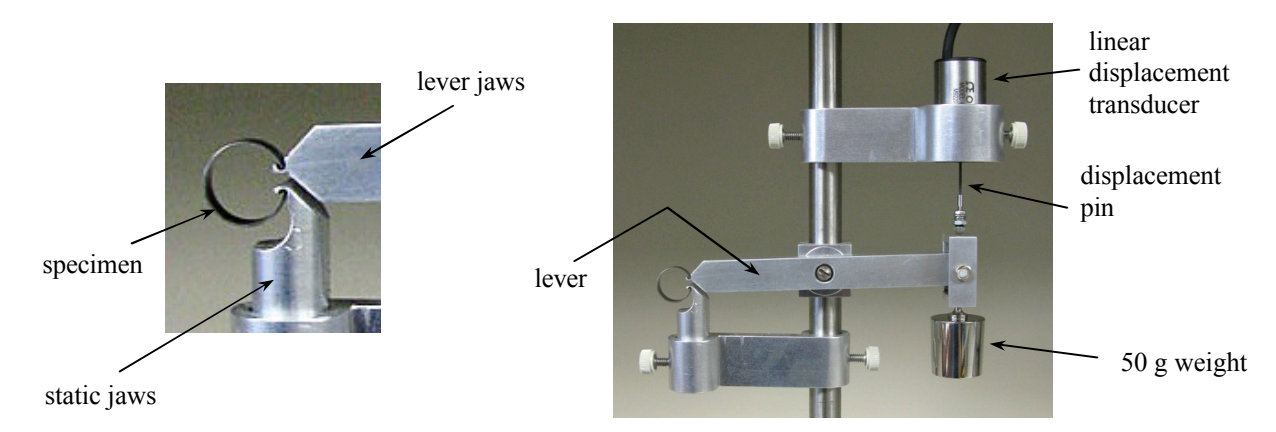


Figure 6: Slotted ring specimen post experiment deflection tester

recorded and transformed the transducer voltage signal to a deflection distance. Eq. (6) is an analytical equation relating the deflection of the slotted ring to the force acting on the ring where R (m) is the ring radius, F_y (N) is the weight force, E (Pa) is the Young's modulus, I (m) is the width of the ring and t (m) is the ring wall thickness. Eq. (6) is derived using a unit load method [20] and Eq. (5) [14] can be derived is a similar manner.

$$D_{y} = \frac{36\pi R^3 F_{y}}{E I t^3} \tag{6}$$

Since the deflection is proportional to the inverse cube of the specimen wall thickness, small changes in the specimen wall thickness can be detected with this instrument. For example, if the total deflection measurement resolution is 0.025 mm then the measureable change in the specimen wall thickness (due to cracking or erosion), using Eq. (6), is 7.3 μ m (or about 1.8% of the specimen wall thickness).

3. Results

Specimens of Type-1 and Type-2 (Table 1) were tested for their deflection and compared for three different test conditions: (A) Specimens that were exposed to heat only; (B) Specimens exposed to heat and an iodine vapor; and (C) Specimens exposed to heat, iodine vapor with a UO_{2+x} and graphite mixture or oxygen gas additive. Specimens of Type-1 were stressed with a static wedge (ST) and specimens of Type-2 were stressed with static and sliding wedges (SW) (where indicated). Generally, SWs were coated with graphite and STs were not, where indicated.

3.1 Deflection measurements of Type-1 slotted rings

Deflection measurements of Type-1 slotted rings, which were subjected to the three testing conditions are shown in Figure 7. The amount of iodine used is given per unit of surface area of Zircaloy material (i.e., specimen and wedge(s)) in the glass ampoule. In these experiments (Figure 7), three specimens were placed in each ampoule, except for Tests 4 and 7, which contained six specimens per ampoule.

In Test 15, where only heat was applied (A), the average deflection of the specimens was 0.76 ± 0.04 mm (green bar in Figure 7). Assessing the analytical deflection using Eq. (6), where $R=7.55\pm0.13$ mm, $F_y=0.441\pm0.001$ N, $E=97\pm2$ GPa [15], $l=5.0\pm0.1$ mm, and $t=0.40\pm0.01$ mm then $D_y=0.69\pm0.12$ mm, agrees with the measured value from Test 15 within the given error.

In test condition (B), for Tests 4 and 7 (orange bars in Figure 7), where heat and 4.5 ± 0.2 mg cm⁻² iodine were introduced, a slight increase in specimen deflection to ~0.80±0.04 mm was noted. In addition, one out of six specimens failed (cracked in-two) in Test 4. The amount of vacuum-baked graphite per total Zircaloy surface area is also indicated in Figure 7. In Test 7 all the Zircaloy surfaces where coated with 0.4 mg cm⁻² graphite (where it was assumed the layer was 5 μ m thick and 0.9 g cm⁻³ dense [7]) except for the areas immediately opposite the specimen ring slots (regions of maximum stress). The purpose of this test was to promote failures and test if the graphite layer would act as a barrier to iodine; however, no specimens failed. Visually, the surfaces that were graphite coated showed less pitting-etching than surfaces that were not coated. When the iodine content was increased to 28.2±1.0 g cm⁻² (Test 13), the deflection increased further to 0.87±0.04 mm and one out of three specimens failed.

In test condition (C) (blue bar in Figure 7), heat, iodine and a UO_{2+x} with vacuum-baked graphite mixture (Figure 5) were introduced in Tests 21, 24 and 29. The graphite quantity in these tests was about thirty times that of Test 7 and none of the Zircaloy surfaces were coated. The amount of hyperstoichiometric oxygen in the UO_{2+x} is expressed as available moles of O_2 per Zircaloy

surface area. In Tests 21 and 29, which had similar iodine content $(6.4\pm0.3~\text{mg cm}^{-2})$ and dissimilar oxygen source content $((0.40\pm0.01)\times10^{-6}~\text{and}~(1.61\pm0.05)\times10^{-6}~\text{mol cm}^{-2},$ respectively), all specimens failed. When the iodine content increased to $28.2\pm1.0~\text{mg cm}^{-2}$ (Test 24), all specimens remained intact and yielded the highest average deflection $(0.99\pm0.05~\text{mm})$. text

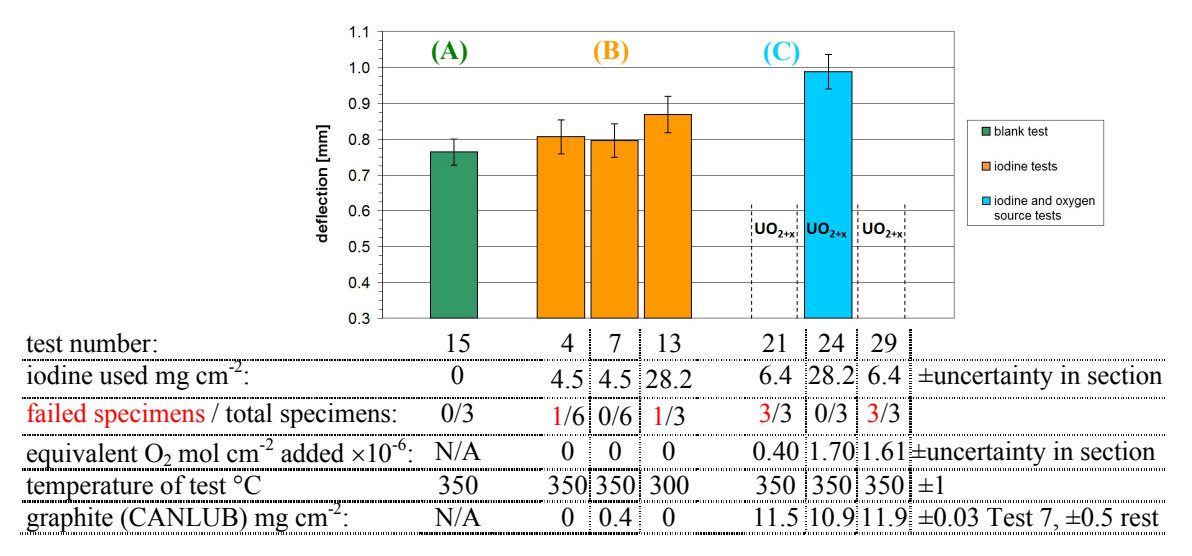


Figure 7: Deflection measurements of Type-1 slotted rings for three test conditions

3.2 Deflection measurements of Type-2 slotted rings

Deflection measurements of Type-2 slotted rings subjected to the three testing conditions are shown in Figure 8. In these tests, all specimens remained intact, but deflection differences were observed. For test condition (A) (heat treatment at $350\pm1^{\circ}$ C), the average deflections of Tests 8 and 18 were 0.48 ± 0.02 mm (green bars, Figure 8). For samples heated at $300\pm1^{\circ}$ C (Test 17), the average deflection was 0.46 ± 0.02 mm. Using Eq. (6), where $R=6.35\pm0.03$ mm, $F=0.441\pm0.001$ N, $E=97\pm2$ GPa [15], $l=5.0\pm0.1$ mm and $t=0.40\pm0.01$ mm, the analytical deflection was $D_v=0.41\pm0.05$ mm, which is within the error of Tests 8, 17 and 18.

For test condition (B) (orange bars, Figure 8), the high iodine concentration (30.0±0.4 mg cm⁻²) used in Tests 19 and 20b yielded an average deflection of 0.96±0.05 mm. This value is comparable to that found in the Type-1 specimens (0.87±0.04 mm, Test 13), where the iodine concentration is comparably high (28.1±1.0 mg cm⁻²). For low to moderate iodine concentrations (4.2±0.2 and 16.0±0.2 mg cm⁻², Tests 3 and 16), the average deflections were 0.49±0.02 and 0.69±0.03 mm, respectively. Similar deflections experienced in Test 3 and in the blank tests (8, 7 and 18) suggest that a possible threshold iodine concentration is required to compromise the structural integrity of the ring specimens (when a SW was used). In Tests 16, 19 and 20b, the results follow a fairly linear relationship between specimen deflection and iodine concentration.

Test condition (C) (blue bars, Figure 8) considers the deflections of specimens exposed to iodine and oxygen, the latter provided by two different sources (i.e., oxygen gas for Tests 20 and 30,

and UO_{2+x} and dried graphite for Test 25). In general, the inclusion of an oxygen source with iodine decreased the average specimen deflections compared with deflections incurred by specimens exposed to iodine only. For instance, in Test 30, the highest iodine concentration mg cm⁻²) (35.5 ± 0.7) combined with significant oxygen concentration a ((8.74±1.22)×10⁻⁶ mol cm⁻²) yielded an average specimen deflection of only 0.70±0.04 mm. This value is much lower than deflections incurred with a comparable amount of iodine alone (i.e., 0.96±0.05 mm in Tests 19 and 20b), suggesting that oxygen has a protective quality on Type-2 specimens in an iodine environment. For a moderately high iodine concentration $(22.1\pm0.3 \text{ mg cm}^{-2})$ and a low concentration of equivalent O_2 ($(0.69\pm0.09)\times10^{-6}$ mol cm⁻²), the deflection also decreased but less drastically (0.82±0.04 mm, Test 20). This suggests that even low concentrations of oxygen gas may contribute to lower specimen deflection. Finally, a moderate oxygen concentration supplied through UO_{2+x} ((1.10±0.01)×10⁻⁶ mol cm⁻²) and graphite additive (8.8±0.2 mg cm⁻²) appears to be directly responsible for decreased deflections (0.89±0.04 mm, Test 25), particularly considering that the iodine concentrations in Tests 19, 20b and 25, are equal (30.0±0.4 mg cm⁻²). Consequently, the addition of oxygen, regardless of its source, appears to protect Type-2 specimens from iodine corrosion.

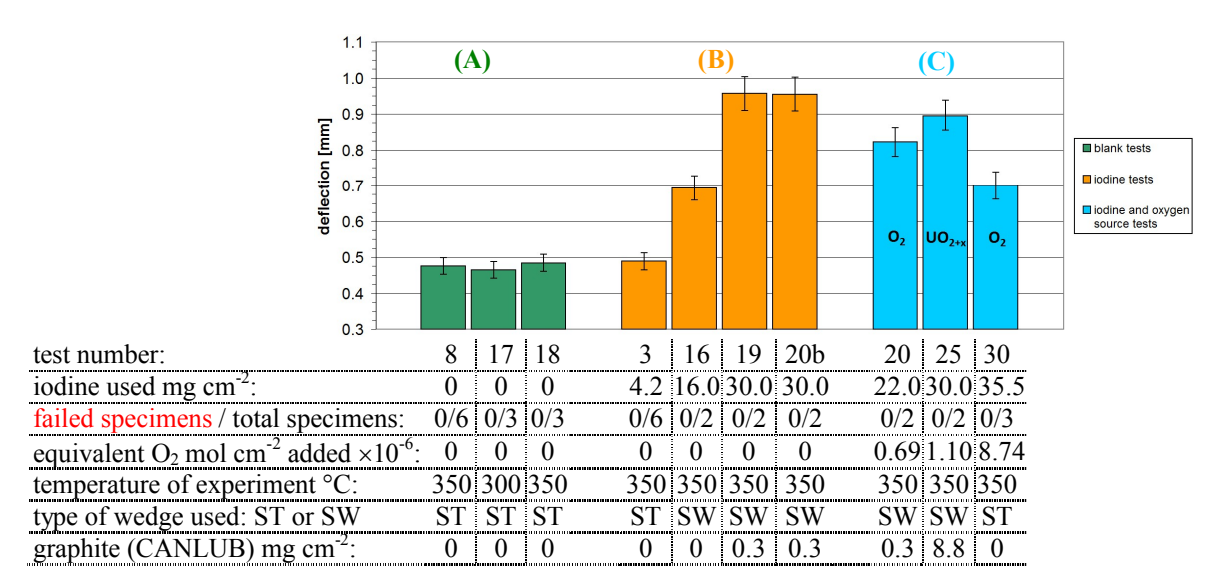


Figure 8: Deflection measurements of Type-2 slotted rings for three test conditions

Lastly, it is mentioned that a small amount of graphite coating (0.34±0.01 mg cm⁻²) was applied to the SW surfaces in Tests 19, 20b, 20 and 25. This was done for the reason mentioned earlier (in Test 7) that perhaps the coating acts as a barrier to iodine, and that the reaction with the Zircaloy wedges would be reduced. Visually, the graphite coated surfaces of the wedges showed somewhat less pitting-etching by the iodine than surfaces that were not coated.

3.3 Effect of iodine vapor residence time

Once the iodine sufficiently reacted with the zirconium to form ZrI_x compounds, the partial pressure of I_2 decreased to a level where the purple iodine vapor colour disappeared. The time

required for this transition may provide insight into structural integrity and/or the oxide thickness. This *iodine residence time* is plotted in the following bar charts:

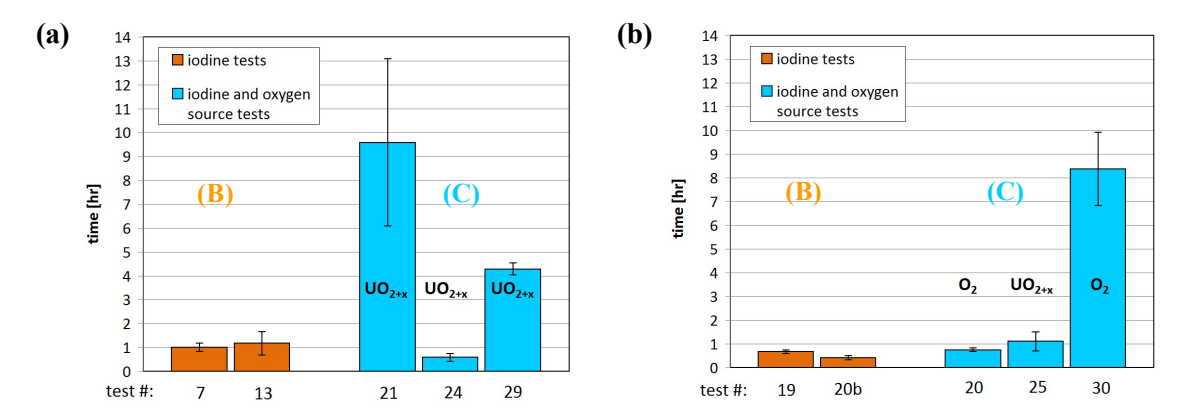


Figure 9: The visible iodine vapor residence time in glass ampoule for: (a) Type-1 sheath specimens; and (b) Type-2 sheath specimens for two test conditions

For the Type-1 specimens, Figure 9a, when only iodine was used in Tests 7 and 13, the iodine vapor residence time was approximately one hour. When the UO_{2+x} and graphite mixture was added, the iodine vapor residence time in Tests 21 and 29 increased to 9.5 ± 3.5 and 4.5 ± 0.3 hrs, respectively. In both cases, only 6.4 ± 0.3 mg cm⁻² of iodine was used and all specimens failed. In Test 24, when the iodine was increased to 28.2 ± 1.0 mg cm⁻² the iodine residence time dropped substantially to only 0.8 ± 0.2 hours and none of the specimens failed, indicating perhaps that iodine corrosion is outpacing oxide layer repair. When all the iodine had been visually converted to ZrI_x species, cracking did not seem to occur. These results suggest (and Figure 7) that a sufficient partial pressure of iodine is required for a minimum amount of time to cause cracking (increased *iodine residence time*).

For Type-2 slotted ring specimens, the iodine vapor residence times were different (Figure 9b). In Test 20, when oxygen gas was added and SWs were used (which is believed to disturb the protective oxide in-situ), the iodine residence time was similar to when no oxygen was present in Tests 19 and 20b (0.4-0.6 hours). In Test 30, the iodine residence time increased to 8.5±1.5 h when the oxygen gas concentration increased by approximately an order of magnitude and a ST was used. In Test 25, which used a UO_{2+x} and graphite mixture and SWs, there was a slight increase in the iodine residence time compared to tests with no oxygen source (1.1±0.4 h versus 0.5±0.1 h), indicating a possible hyperstoichiometric oxygen threshold. Tests 25 and 30 seem to support the deflection measurements seen earlier, indicating the presence of a protective oxide layer between the iodine corrodant and bare zirconium in the radially basal-textured Zircaloy sheath specimens. The corresponding oxygen concentrations for these tests are outlined in Figure 8.

3.4 Effect of corrosion on wall thickness

The slotted-ring wall thickness, t, was measured with a digital Mastercraft (150 mm span) caliper after performing the experiments for the three test cases. Measurements were taken at the centre

and edges of the specimens (Figure 1b). The wall thicknesses of Type-1 and Type-2 slotted ring specimens, in Figure 10a and Figure 10b, are shown, respectively.

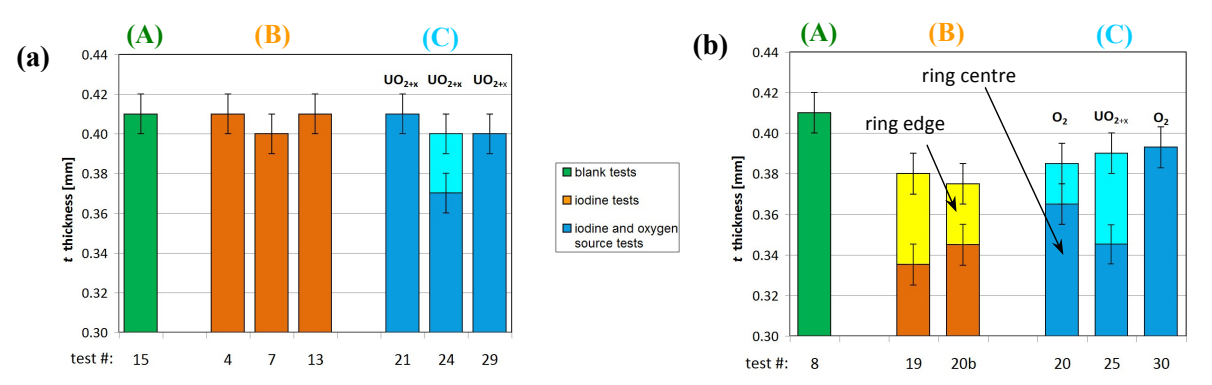


Figure 10: The slotted ring specimen wall thickness t vs. test number for: (a) Type-1 specimens; and (b) Type-2 specimens at specimen centres, for three test conditions, where yellow and light blue bars indicate wall thicknesses at specimen edges

The wall thicknesses of Type-1 specimens remained statistically equal (≈0.40 mm) for all three testing conditions (Figure 10a). However, in Test 24, there was a marked erosion of the surface when a higher iodine concentration was used (where the dark and light color bars represent the specimen thicknesses at centre and edge of the specimen, respectively). For Type-2 specimens, Figure 10b, there was a marked corrosion of surfaces for the iodine-only experiments. Specifically, in Tests 19 and 20b, where 30.0±0.4 mg cm⁻² of iodine was used, most of the iodine-induced corrosion occurred at the centre of the specimen where the stress was highest (orange bars) and less where stress was lower (yellow bars). The corroded materials from specimen surfaces are revealed as orange-brown deposits in the glass ampoule away from the specimen and wedges. These deposits were later identified (using EDX and NAA) as composed of Zr and I with a Zr:I atomic ratio of about ~1:2, indicating ZrI₂ deposits or possibly ZrI+ZrI₃ deposits as described by the Zr-I phase diagram by Lewis and Kleczek *et al.* [7].

The calculated deflection (using Eq. (6)) of Test 19 is D_y =0.70±0.12 mm, where the minimum average measured t value is 0.34±0.01 mm (from Figure 10b), R=6.35±0.03 mm, F=0.441±0.001 N, E=97±2 GPa [15], and l =5.0±0.2 mm. The actual average deflection of Test 19 was 0.96±0.05 mm in Figure 8, which does not agree with the calculated value. Hence, it is possible that the specimen degradation is a combination of both external and internal corrosion (the latter possibly being cracks). In Test 30, where oxygen was added, the specimen average wall thickness was 0.39±0.01 mm, and there was no increased corrosion at the specimen centre. Since the deflection in Test 30 (Figure 8) was also the lowest measured, this result supports the observations that increased oxygen concentration helps to repair or restore the ZrO_2 protective layer in Type-2 specimens.

4. Summary

4.1 Type-1 specimens

Type-1 specimens exposed to iodine vapor at 350°C experienced a failure rate of 13% (Figure 7). In a test that included graphite coating (CANLUB) on all Zircaloy surfaces, except for areas of maximum tensile stress (where cracking was expected to occur) no failures occurred. In this test the graphite coating also seemed to reduce pitting-etching of the covered surfaces. Thus, this result does not support the idea of a completely impenetrable graphite coating barrier to iodine but it may support a gettering or an absorptive process. For moderate iodine concentrations (\approx 6.4 mg cm⁻²), the addition of a UO_{2+x} and graphite mixture increased the iodine vapor residence time from less than an hour to several hours, and all specimens failed. Although the additives likely increased the thickness of the zirconium oxide layer, which would largely prevent iodine-zirconium contact, irregularities in the oxide layer caused by the specimen texture [21] are believed to have led to specimen failure.

Although increased iodine content caused surface degradation in Test 24, no failures were observed. At high iodine concentrations, the residence time for the reactive iodine species was less than an hour. This suggests that there is a complex time-dependent interaction between the iodine, zirconium, and oxide, which requires further investigation. This suggested further work may give more insight into the corrosion processes in Type-2 specimens (which are more representative of current sheathing).

4.2 Type-2 specimens

Type-2 specimens exposed to iodine above a critical level (≈4 mg cm⁻²) remained intact, but increased specimen deflections were measured. The introduction of oxygen gas (leading possibly to oxide layer build-up and repair) was shown to be effective in protecting these Zircalov specimens (even when the highest amount of iodine was used).

When UO_{2+x} and graphite mixture additive was introduced, there was a slight decrease in the average deflection and a slight increase in iodine residence time (i.e., less corrosion). This indicates that oxygen, from UO_{2+x} , may have oxide-repairing properties for Type-2 specimens. As Type-2 specimens are more representative of current sheathing material, further investigation of the mechanism for oxide repair is also useful.

4.3 Influence of texture on specimen failure rate

Type-1 specimens showed a more consistent and decisive failure rate than did Type-2 specimens (Figure 7 and Figure 8). Kim *et al.* [21] offer a possible explanation for the different I-SCC behaviour. They suggested that unalloyed zirconium texture containing prism planes parallel to specimen surfaces (similar to Type-1 specimens but which also had pyramidal planes) has two or more oxide growth planes, whereas zirconium texture with basal planes parallel to specimen surfaces (similar to Type-2 specimens) has only one oxide growth plane. Therefore, the Type-2

specimen texture is likely more resistant to corrosion, as a thick and continuous 'columnar' oxide layer in the zirconium oxide provides superior surface protection [21].

5. Conclusions and Future Work

Specimen deflection measurements and failures (Figures 7 and 8), iodine residence times (Figure 9), and specimen thickness measurements (Figure 10) suggest that adding oxygen (from either O_2 or UO_{2+x}) provides some protection from iodine corrosion. The graphite addition appears to be an integral part of the oxide repair mechanism. Therefore, confirmatory I-SCC tests with an oxygen addition, including varying quantities of graphite, will be conducted in an attempt to better understand the key processes at work. In addition, further tests will focus on determining the absorptive nature of the graphite impurities to iodine species as proposed in Ref. [7] and investigate its barrier properties to iodine as well.

6. Acknowledgements

These studies were performed at the Royal Military College of Canada, Kingston, Ontario. The authors would like to thank Dr. W.T. Thompson for his advice on chemistry thermodynamics, thank senior technologists Mr. T. Nash, Mr. B. Ball, Mr. C. McEwen and Mr. B. Whitehead for their invaluable technical support and thank Mr. B.A. Surette at Chalk River Laboratories for his advice. Thanks also go out to Dr. P. Chan and Dr. K. Farahani for supplying additional test materials and general assistance.

7. References

- [1] P.S. Sidky, "Iodine stress corrosion cracking of Zircaloy reactor cladding: iodine chemistry (a review)", *Journal of Nuclear Materials*, 256 (1998) 1-17.
- [2] B. Cox, "Pellet-clad interaction (PCI) failures of zirconium alloy fuel cladding A review", *Journal of Nuclear Materials*, 172 (1990) 249-292.
- [3] K. Edsinger and K.L. Murty, "LWR Pellet-Cladding Interactions: Materials Solutions to SCC", *Journal of the Minerals and Materials Society*, (2001), 9-13.
- [4] S.H. Shann and D.R. Olander, "Stress corrosion cracking of Zircaloy by cadmium, iodine and metal iodides", *Journal of Nuclear Materials*, 113 (1983) 234-248.
- [5] B. Cox, "Stress corrosion cracking of zirconium alloys", *Journal of the American Chemical Society*, 3 (1987) 867-873.
- [6] B. Cox, B.A. Surette and J.C. Wood, Stress corrosion cracking in unirradiated and irradiated CsI, *Journal of Nuclear Materials*, 138 (1986) 89-98.
- [7] B.J. Lewis, W.T. Thompson, M.R. Kleczek, K. Shaheen, M. Juhas, and F.C. Iglesias, Modelling of iodine-induced corrosion cracking in CANDU fuel, *Journal of Nuclear Materials*, 408 (2011) 209-223.
- [8] J.C. Wood, B.A. Surette and I. Aitchison, "Pellet cladding interaction Evaluation of lubrication by graphite", *Journal of Nuclear Materials*, 88 (1980) 81-94.
- [9] L. Fournier, A. Serres, Q. Auzoux, D. Leboulch and G.S. Was, "Proton irradiation effect on microstructure, strain localization and iodine-induced stress corrosion cracking in Zircaloy-4", *Journal of Nuclear Materials*, 384 (2009) 38-47.

- [10] K. Une, Stress corrosion cracking in of Zircaloy-2 cladding in iodine vapor, *Journal of Nuclear Science and Technology*, 14 (1977) 443-451.
- [11] P.G. Lucuta, Hj. Matzke and R.A. Verrall, "Thermal conductivity of hyperstoichiometric SIMFUEL", *Journal of Nuclear Materials*, 223 (1995) 51-60.
- [12] J.J. Katz and E. Rabinowitch, <u>The chemistry of uranium: The element, its binary and related compounds</u>. Dover Publications Inc., New York, 1951.
- [13] C.W. Bale, P. Chartrand, S.A. Degterov, G. Eriksson, K. Hack, R. Ben Mahfoud, J. Melancon, A.D. Pelton and S, Petersen, FactSage Thermochemical Software and Databases, *Calphad*, 26, No. 2 (2002) 189-228.
- [14] J.C. Wood, "Factors affecting stress corrosion cracking on Zircaloy in iodine vapor", Journal of Nuclear Materials, 45 (1972) 105-122.
- [15] H.E. Rosinger, "The elastic properties of zirconium alloy fuel cladding and pressure tubing materials", *Journal of Nuclear Materials*, 79 (1979) 170-179.
- [16] R. Kaufmann, H. Klewe-Nebenius, H. Moers, G. Pfennig, H. Jennet and H.J. Ache, XPS Studies of the Thermal Behaviour of passivated Zircaloy-4 surfaces, *Surface and Interface Analysis*, 11 (1988) 502-509.
- [17] M. Peehs, H. Stehle and E. Steinberg, Out-of-pile testing of iodine stress corrosion cracking in Zircaloy tubing in relation to pellet-cladding interaction phenomenon, *Zirconium in the Nuclear Industry* 4th Conference, ASTM STP 681, Philadelphia, PA, 1979, 244-260.
- [18] E. Tenckhoff, Deformation Mechanism, Texture and Anisotropy in Zirconium and Zircaloy, ASTM, STP-966, ASTM, 1988.
- [19] T. Yang and C. Tsai, "On the susceptibility to stress corrosion cracking of Zircaloy in an iodine containing environment", *Journal of Nuclear Materials*, 166 (1989) 252.
- [20] R.D. Cook and W.C. Young, <u>Advanced Mechanics of Materials 2nd Ed</u>. Prentice Hall New Jersey, 1999.
- [21] H.G. Kim, T.H. Kim and Y.H. Jeong, "Oxidation characteristics of basal (0002) plane and prism (1120) plane in HCP Zr", *Journal of Nuclear Materials*, 306 (2002) 44-53.